REVIEW ARTICLE | INSIGHT
https://doi.org/10.1038/s41567-021-01403-z

nature physics

Quantum gases in optical boxes

Nir Navon[1], Robert P. Smith[2] and Zoran Hadzibabic[3]✉

Quantum atomic and molecular gases are flexible systems for studies of fundamental many-body physics. They have traditionally been produced in harmonic electromagnetic traps and thus had inhomogeneous densities, but recent advances in light shaping for optical trapping of neutral particles have led to the development of flat-bottomed optical box traps, allowing the creation of homogeneous samples. Box trapping simplifies the interpretation of experimental results, provides more direct connections with theory and, in some cases, allows qualitatively new, hitherto impossible experiments. It has now been achieved for both Bose and Fermi atomic gases in various dimensionalities, and also for gases of heteronuclear molecules. Here we review these developments and the consequent breakthroughs in the study of both equilibrium and non-equilibrium phenomena such as superfluidity, turbulence and the dynamics of phase transitions.

Since the earliest days of ultracold atomic gases, their successful use in studying many-body physics[1–3] has owed a lot to the possibility of trapping the atoms in versatile potentials, including low-dimensional traps[4], double wells[5] and optical lattices[6–8]. The electromagnetic trapping potentials are often also dynamically tuneable, which has allowed experiments ranging from studies of elementary excitations[9–11] to reversible crossing of phase transitions[12,13].

More recent advances in the shaping of optical potentials have opened many new possibilities. One major development is the increasingly popular use of the uniform (flat-bottom) optical box traps[14–19], as opposed to the traditionally used (optical or magnetic) harmonic ones. Box traps have allowed scientific breakthroughs in a wide range of areas, including studies of superfluidity, turbulence and the dynamics of phase transitions. For example, the gas homogeneity has been beneficial for measurements of density-dependent quantities, such as the speeds of different types of sound in various superfluids[20–27], quantum depletion in a condensed Bose gas[28] or the pairing gap in a Fermi gas[29,30]. Qualitatively new observations have also been made, such as recurrences in closed quantum systems[31], the unexpected observation of the quantum Joule–Thomson effect[32] or the discovery of a novel type of breather[33].

In this Review, we describe the development of box traps and the scientific successes in this new and growing field. Before starting, we also draw the reader's attention to contemporary reviews on two related emerging fields: (1) the creation of 'atomtronics' circuits for coherent matter waves, such as ring traps that support persistent currents[34], and (2) the trapping of individual atoms or molecules in arrays of optical tweezers[35]. All three fields take advantage of advances in light shaping, and there are also scientific connections; as a prominent example, the dynamics of phase transitions in a homogeneous system have been studied in ring traps[36], two-dimensional (2D) and three-dimensional (3D) box traps[15,37] and a one-dimensional (1D) tweezer array[38].

Making box traps

The basic concept behind most box traps is using sculpted repulsive (blue-detuned) laser beams to construct the box walls that confine the particles (Fig. 1a). Three-dimensional box traps are most commonly cylindrical and are made using one hollow-tube beam and two sheet end-cap beams. To make a homogeneous 3D potential, one also levitates the particles against gravity, which for atoms is usually done using a static magnetic field gradient[14], whereas polar molecules can be levitated using a static electric field gradient[19]. To make a low-dimensional box, one freezes out the particle motion along some direction(s) using very tight confinement, which can be harmonic; this dimensionality reduction is analogous to the making of a low-dimensional harmonic trap[4]. One could also make red-detuned (attractive) box traps, and also cancel gravity using a light field of linearly varying intensity[39], but this is technically more demanding because of the need to sculpt high-intensity light such that the variations in the optical potential are smaller than all the relevant energy scales in the gas.

The development of optical boxes was greatly aided by two complementary types of programmable spatial light modulator (SLM)—the liquid-crystal SLMs that modulate the phase of laser beams and the digital micromirror devices (DMDs) that modulate their amplitude (Fig. 1b). A liquid-crystal SLM is a rectangular array of ~10^6 pixel elements (each ~10 μm in size) with individually controllable indices of refraction; using it to imprint a spatially modulated phase delay on a laser beam, one controls the intensity pattern in the vicinity of the conjugate (Fourier) plane. Similarly, a DMD is a rectangular array of ~10^6 mirrors (each ~10 μm in size) that can be individually turned 'on' or 'off' (by changing their tilt angle) to spatially modulate the amplitude of a beam. An arbitrary intensity pattern can then be imaged onto the cloud[40].

Liquid-crystal SLMs are convenient for creating the multiple beams needed for a box trap using a single device[14], and are generally more power-efficient than DMDs. On the other hand, DMDs are more convenient for making arbitrarily shaped boxes, such as squares in 2D or cubes in 3D, and much better for creating dynamical potentials. Owing to their subkilohertz refresh rate at present, liquid-crystal SLMs cannot be reprogrammed during an experimental run without the particles escaping while the phase pattern is being updated and the trap temporarily turned off. Meanwhile, the ~10 kHz refresh rate of DMDs is sufficiently high for the trapping pattern to be dynamically changed without the ultracold particles moving noticeably during the updates[41].

The versatility of SLMs has been essential for experimental exploration[42], but box walls can also be made using non-tuneable tools, such as axicons[17,18,43] and custom-manufactured masks[15], which can be more cost-effective and power-efficient. Yet another option is to use 'painted' time-averaged potentials created by fast spatial scanning of laser beams[44]. For a comprehensive review of recent advances in light shaping for atom trapping, including comparisons of different methods, see ref. [41].

Using the various light-sculpting methods, boxes of various shapes and dimensionalities have been created for both atomic and molecular gases[14–19], as illustrated in Fig. 1c; see also refs. [45–48] for

[1]Department of Physics, Yale University, New Haven, CT, USA. [2]Clarendon Laboratory, University of Oxford, Oxford, UK. [3]Cavendish Laboratory, University of Cambridge, Cambridge, UK. ✉e-mail: zh10001@cam.ac.uk

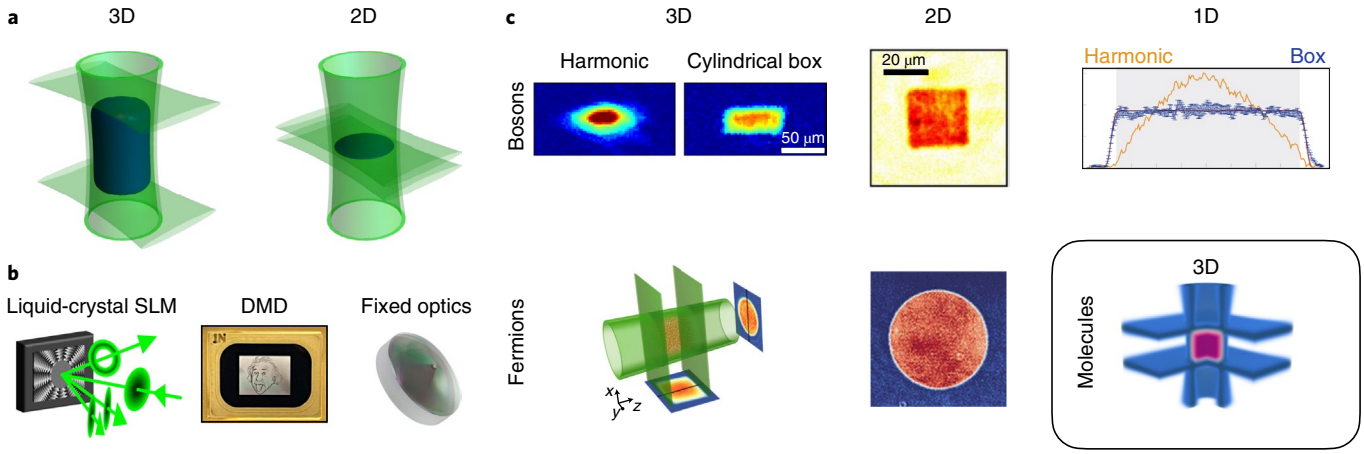

Fig. 1 | Optical box traps. a, The concept. The walls of the box are made using repulsive laser beams (green) and the particles (blue) are confined in the dark region between them. Here, a cylindrical 3D box is sculpted using one hollow-tube beam and two end-cap beams. A 2D box is made by freezing out the particle motion in one direction (vertical, in this case) using very tight confinement. To create a 1D box, one freezes out the motion in two directions. **b**, The box tools. Programmable spatial light modulators (SLMs)—the phase-controlling liquid-crystal SLM (left) and the amplitude-controlling digital micromirror device (DMD) (middle)—offer great flexibility for sculpting laser beams. In the cartoon, starting with a single Gaussian beam, a single liquid-crystal SLM is used to create all three beams for a cylindrical 3D box[14]. Right: box traps can also be made using specialized fixed optics, such as an axicon, to create a tube beam. **c**, Box trap gallery. Between 2013 and 2021, optical boxes have been realized for Bose and Fermi atoms in various dimensionalities, as well as for (fermionic) heteronuclear molecules in 3D[14–19]. Panels adapted with permission from: **b** (left), **c** (top left pair), ref. [14], APS; **c** (top middle), ref. [15], Springer Nature Ltd; **c** (top right), ref. [16] under a Creative Commons License CC BY 4.0; **c** (bottom left), ref. [17], APS; **c** (bottom middle), ref. [18], under a Creative Commons License CC BY 4.0; **c** (bottom right), ref. [19] under a Creative Commons License CC BY 4.0.

earlier examples of confining laser-cooled atoms with blue-detuned beams and refs. [49,50] for early prototypes of 1D box traps.

As a final point in this section, optical box traps are not perfect. The sharpness of their walls is limited by the optical wavelength of ~1 μm, which is not negligible compared with the typical box dimensions of 10–100 μm. Moreover, additional fields used for levitation, the creation of low-dimensional gases[15,16,51] or tuning of interactions can lead to further imperfections. In Box 1, we discuss two complementary methods used to quantify the uniformity of box-trapped gases. The uniformity achieved so far has been good enough for the success stories we discuss in the next section, but how close to perfect a box needs to be ultimately depends on the specific scientific problem (see the 'Outlook' section).

Success stories

Here we outline the scientific advances afforded by homogeneous atomic gases, which also illustrate the general types of problem for which box traps are advantageous.

Quantum statistics. We start with experiments on purely quantum-statistical phenomena (Fig. 2). In harmonic traps, the real and momentum space are coupled such that, for example, one can clearly observe real-space effects of Bose–Einstein condensation (BEC)[52] and Fermi pressure[53]. In a box trap, the signatures of quantum statistics are harder to see in real space (Fig. 2a), but in momentum space they are revealed more cleanly than in harmonic-trap experiments (Fig. 2b).

For bosons, one clearly observes the statistical nature of the BEC transition, which is driven by the saturation of the total occupation of all excited (momentum) states[32]. As the total atom number in the gas is increased at a fixed temperature, the number of atoms in the thermal cloud saturates at the critical value for condensation and all the extra atoms accumulate in the condensate; in harmonic traps this textbook effect is obscured by a combination of geometric and mean-field interaction effects[54].

For fermions, one instead observes the occupation-number saturation at the level of individual momentum states, as prescribed by the Pauli exclusion principle. Here, the occupation of a state corresponding to a momentum $\mathbf{k}$ is denoted n_k. As the temperature (normalized to the Fermi temperature T_F) is reduced, the occupation of

Box 1 | Characterizing box traps

a, One simple measure of the gas homogeneity is the distribution of the real-space densities. Here we show the distribution of column densities, n_{2D}, extracted from in situ images of 3D clouds[17]. In a box trap (blue) the probability distribution $\mathcal{P}(n_{2D})$ is narrow, strongly peaked near the average value $\overline{n_{2D}}$. This means, for example, that most atoms experience essentially the same mean-field potential. For comparison, the corresponding distribution in a non-degenerate harmonically trapped gas (red) is very broad; the expected distribution is uniform between 0 and $2\overline{n_{2D}}$. **b**, A complementary characteristic of box traps is the single-particle density of states, which is seen (for example) in the dependence of the critical atom number for Bose–Einstein condensation, N_c, on the temperature, T (ref. [32]). In a 3D harmonic trap $N_c \propto T^3$, whereas in a perfect 3D box $N_c \propto T^{3/2}$. Here the experimental data are captured by $N_c \propto T^{\alpha}$ with $\alpha = 1.65$ (red line). A common way[14] to characterize (imperfect) box traps is to model them by an isotropic power-law potential $V(\mathbf{r}) \propto r^p$, with $p \gg 1$. Then $\alpha = 3/2 + 3/p$, and for a Fermi gas one similarly gets that the Fermi energy is[17] $E_F \propto N^{1/\alpha}$. In current experiments $p > 10$ is readily achieved, and there are indications that values of p up to ~100 are feasible[18].

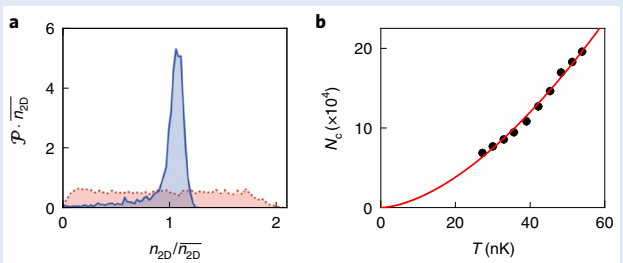

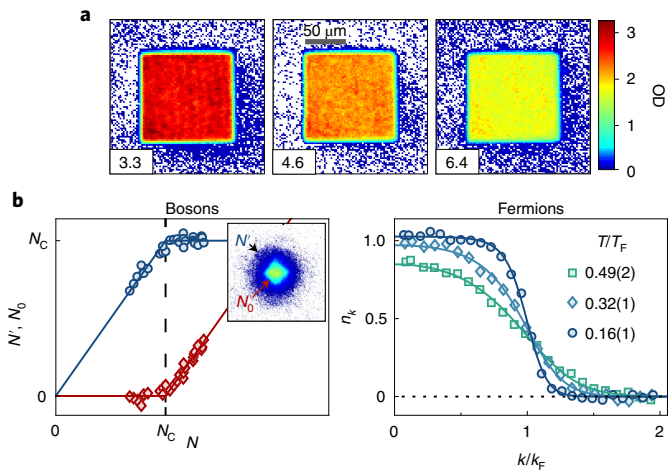

Fig. 2 | Quantum statistics in homogeneous gases. a, In situ absorption images of homogeneous quantum-degenerate 3D gases with different phase-space densities $\mathcal{D} > 1$ (indicated in the bottom-left corners); the colourscale bar shows the optical density (OD) and applies to all three panels. The gas with lowest density (lowest OD) is the coldest and actually has the highest $\mathcal{D}$. However, one cannot see this, or even whether the gases are fermionic or bosonic (here they are fermionic ^{6}Li gases; original data collected by N.N.'s group), in the images. **b**, In contrast, the effects of quantum statistics and degeneracy are striking in momentum space. Left: for a Bose gas, the statistical nature of the BEC phase transition, driven by the saturation of the excited states, is revealed more clearly than in the corresponding harmonic-trap experiments[54]. Here the plot shows the total number of atoms in the thermal cloud (N', blue symbols and line) and the condensate (N_0, red symbols and line), as the number of atoms in the cloud (N) is varied at constant temperature[32]; the inset shows an image of a partially condensed gas after release from the box and free expansion (original data collected by Z.H.'s group). Right: for a Fermi gas below T_F, the effects of the Pauli exclusion principle are clearly observed. The occupation of individual momentum states is limited to $n_k \lesssim 1$, and the Fermi surface forms at $\mathbf{k}_F$. All solid lines are based on ideal-gas theory. In the right panel, the numbers in the parentheses show fitting errors. Panel **b** (right) adapted with permission from ref. [17], APS.

all states remains bound to $n_k \lesssim 1$ and the Fermi surface forms[17] at the Fermi wavevector $\mathbf{k}_F$.

Experiments on the thermodynamics of nearly-ideal box-trapped gases also lead to the unexpected observation of the Joule–Thomson effect that arises solely from quantum correlations[32]. While the ideal classical gas does not change temperature under isoenthalpic rarefaction, the ideal Bose gas cools and the ideal Fermi gas is expected to heat[55].

Equilibrium properties of interacting systems. We now move on to the experiments on the many-body physics of interacting gases. We start with the broad class of spectroscopic and transport measurements in which one weakly perturbs a system to extract information on its equilibrium properties (Fig. 3).

A lot of attention has been given to long-wavelength sound waves[20–27]; in Fig. 3a(i), we show examples of sound propagation in 3D Fermi[22] and 2D Bose[21] gases. The key quantities studied in such experiments are the sound speed and the sound attenuation (or equivalently diffusivity). Both of these quantities are density dependent, and the crucial advantage of box traps for interpreting the measurements is that they are constant in space.

In Fig. 3a(ii) we illustrate two scientific highlights of the experiments on sound in homogeneous superfluids. In both 3D and 2D unitary Fermi gases the quantum limit of sound diffusivity, set by $\hbar/m$ (where m is the atom mass), was demonstrated[22,26]; this universal limit should also be relevant for other strongly interacting Fermi systems such as neutron stars. In a weakly interacting 2D Bose gas, first and second sound[56,57] in a Berezinskii–Kosterlitz–Thouless (BKT) superfluid[58,59] were observed for the first time, and the measurements of the two sound speeds revealed the universal superfluid-density jump at the BKT transition[60]. Related experiments on superfluidity have investigated the Josephson effect[61] and the critical velocity[62] in a 2D Fermi gas, whereas a more complex trapping geometry allowed studies of a Bose gas superfluid flow through a constriction between two reservoirs[63].

In Fig. 3b we illustrate the benefits of gas homogeneity for spectroscopic measurements that globally probe the system[28,29,64–69]; for experiments on the extraction of the properties of a homogeneous gas by local probing of harmonically trapped gases, see refs. [70–73].

The Rabi radiofrequency spectra shown in Fig. 3b(i) measure the energy cost of removing a particle from a spin−1/2 3D Fermi gas at different reduced temperatures T/T_F (ref. [66]). Measurements were performed on the whole sample and the spectra taken at closely spaced T/T_F values are clearly distinct thanks only to the lack of inhomogeneous broadening; in a harmonic trap global measurements would mix signals for a wide range of $T/T_F(\mathbf{r}) \propto n(\mathbf{r})^{-2/3}$, where $n(\mathbf{r})$ is the local density. Rabi radiofrequency spectroscopy of 3D Fermi gases[66,67] has, for example, provided an observation of non-Fermi-liquid behaviour in a normal strongly interacting gas[66], whereas Ramsey radiofrequency spectroscopy of 2D Bose gases has provided measurements of short-range correlations across the BKT transition (Fig. 3b(ii)) and an observation of magnetic dipole interactions[68,69].

The lack of inhomogeneous broadening is similarly beneficial for Bragg spectroscopy[74,75]. Figure 3b(iii) shows measurements of the excitation spectrum of a strongly interacting 3D Fermi gas, which were used to extract the concavity of the dispersion relation and the density-dependent pairing gap in the BEC–BCS crossover[29]; see also ref. [30] for similar measurements on 2D Fermi gases. Bragg spectroscopy experiments on condensed homogeneous 3D Bose gases have provided an observation of Heisenberg-limited long-range coherence[64], the confirmation of Bogoliubov's theory of quantum depletion[28] and an observation of the breakdown of Bogoliubov's theory of the excitation spectrum for sufficiently strong interactions[65].

Non-equilibrium phenomena. In another large class of experiments, homogeneous interacting gases have been driven or quenched far from equilibrium (Fig. 4).

One paradigmatic topic in non-equilibrium physics is turbulence in strongly driven systems. Depending on the system and the excitation protocol, turbulent dynamics can be dominated by either waves or vortices, and the advent of box traps has led to new insights in both cases (Fig. 4a).

Wave turbulence is theoretically described in terms of dynamics that are local in momentum space[76], so it is advantageous to experimentally study it in momentum space, for which box traps (with their plane-wave eigenstates) provide the natural setting. In 'shaken' 3D box-trapped Bose gases the power-law momentum distribution characteristic of a direct turbulent cascade has been observed[20], and the elusive particle and energy fluxes through the cascade have also been measured[77].

Vortex dynamics have been studied in turbulent (quasi-)2D box-trapped Bose gases. Such dynamics can arise owing to various reasons, including vortex interactions and density gradients; eliminating the latter allowed clean observations of vortex clustering corresponding to negative temperatures[78,79] (see also refs. [80,81]), as predicted by Onsager in 1949[82]. In another recent experiment on box-trapped 2D Fermi gases, the interplay of accelerated vortices and waves has also been observed[83].

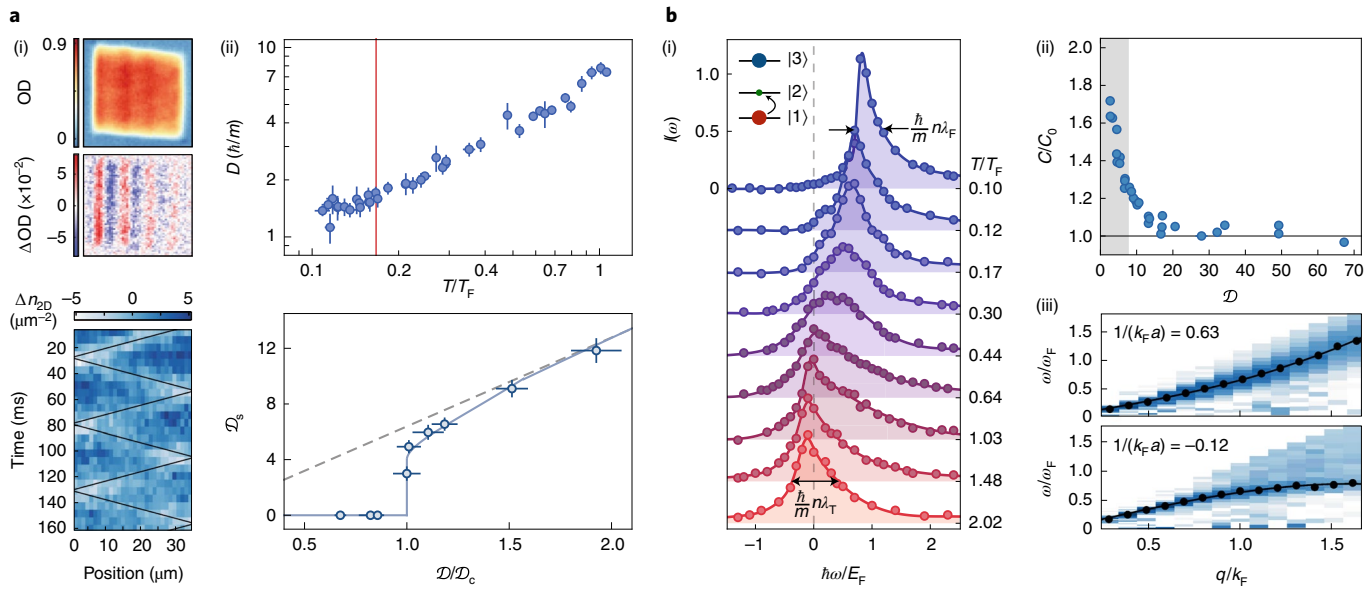

Fig. 3 | Sound and spectroscopy measurements on box-trapped gases. a, Sound measurements: (i) low-energy sound modes can be probed by perturbing the gas with an external potential and observing the evolution of the resulting density modulations in time and space. Images show examples of measurements in a 3D Fermi gas[22] (top; here OD shows the modulated density, and ΔOD the variation around the average value) and a 2D Bose gas[21] (bottom). (ii) top: the sound diffusivity D (seen in the attenuation of the wave) in a low-temperature unitary Fermi gas approaches the universal quantum limit, $D \approx \hbar/m$; the red line indicates T_c, the critical temperature for superfluidity. Bottom: the superfluid phase-space density $\mathcal{D}_s$ in a 2D Bose gas, which was deduced from the measured speeds of first and second sound, undergoes a universal jump from 0 to 4 at the BKT phase transition; $\mathcal{D}_c$ is the critical phase-space density[25]. The solid blue line is the theoretical prediction, whereas the grey dashed line corresponds to a superfluid fraction of 100%. For the error bars, see refs. [22,25]. **b**, Spectroscopy measurements: (i) particle-ejection spectra $I(\omega)$ for the unitary 3D Fermi gas[66]. Rabi radiofrequency (rf) spectroscopy was performed on the whole cloud and the differences induced by small changes in T/T_F are observable only due to the lack of inhomogeneous broadening. Such measurements probe short-range correlations and have also revealed non-Fermi-liquid behaviour in the normal unitary gas at $T > T_c$. Here ω is the rf photon angular frequency, λ_F is the Fermi wavelength, λ_T is the thermal wavelength. As depicted in the cartoon, the gas is prepared in a mixture of states $|1\rangle$ and $|3\rangle$, and the spectroscopy is performed on the $|1\rangle$ to $|2\rangle$ transition. (ii) Ramsey radiofrequency spectroscopy on a 2D Bose gas was used to determine the two-body contact (C) as a function of $\mathcal{D}$; the shaded region indicates the non-superfluid phase. (iii) Bragg spectroscopy was used to measure the excitation spectrum in a strongly interacting 3D Fermi gas, here shown for two values of the interaction parameter $k_F a$, where a is the s-wave scattering length[29]. Panels adapted with permission from: **a**(i) (top), **a**(ii) (top), ref. [22], AAAS; **a**(i) (bottom), ref. [21], APS; **a**(ii) (bottom), ref. [25], Springer Nature Ltd; **b**(i), ref. [66], APS; **b**(ii), ref. [69], Springer Nature Ltd. Panel **b**(iii) courtesy of the authors of ref. [29].

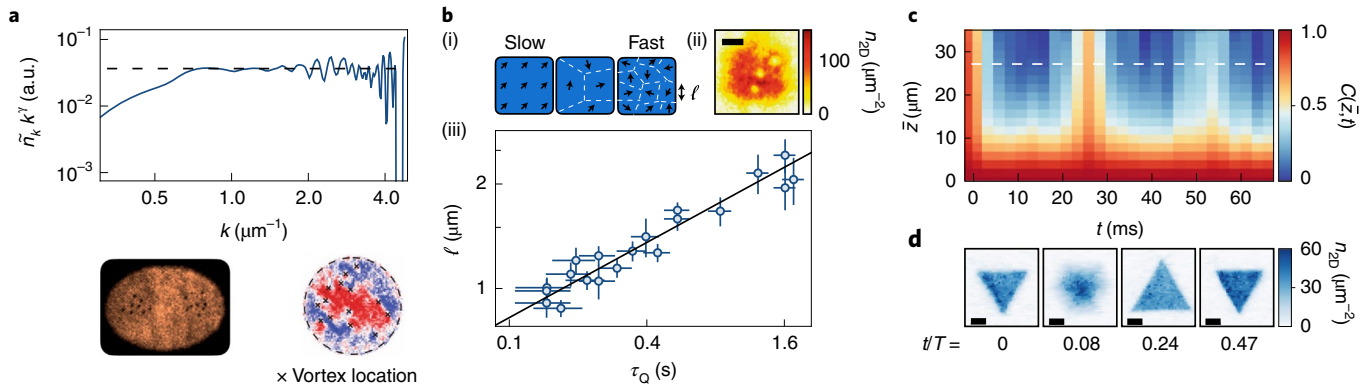

Fig. 4 | Non-equilibrium phenomena. a, Wave and vortex turbulence. Top: power-law momentum distribution ($\tilde{n}_k \propto k^{-\gamma}$, indicated by the dashed line) in a 3D Bose gas driven on a large length scale reveals a wave-turbulence cascade towards smaller length scales[20,77]. a.u., arbitrary units. Bottom: experiments on vortex turbulence in quasi-2D Bose gases showed large-scale vortex clustering, which was observed by probing the density distribution[78] (left) and the superfluid-velocity field[79] (right). **b**, Critical dynamics: (i) critical slowing down results in non-adiabatic crossing of the BEC transition and the formation of domains with different spontaneously chosen condensate phases (indicated by the arrows). (ii) Topological defects form at the domain boundaries; here the image shows vortices spontaneously generated in a quench-cooled gas[15]. (iii) The power-law dependence of the average domain size, ℓ, on the quench time, τ_Q, is in agreement with the Kibble–Zurek theory[37]. **c**, Recurrences of phase correlations were observed in a 1D Bose gas[31]. **d**, A novel breather was seen in a 2D Bose gas; for particular initial density distributions, such as a uniform triangle prepared in a box trap, the cloud evolving in a harmonic potential (with trap frequency $1/T$) periodically returns to its initial state[33]. The scale bars in **b**(ii) and **d** correspond to 10 μm. Panels adapted with permission from: **a** (top), ref. [20], Springer Nature Ltd; **a** (bottom left), ref. [78], AAAS; **a** (bottom right), ref. [79], AAAS; **b**(ii), ref. [15], Springer Nature Ltd; **b**(iii), ref. [37], AAAS; **c**, ref. [31], AAAS; **d**, ref. [33] under a Creative Commons License CC BY 4.0.

Box 2 | Critical phenomena in harmonic and box traps

Box traps are particularly advantageous for studies of phenomena associated with long-range correlations, such as those emerging near second-order phase transitions. Here we illustrate this advantage with a simple ideal-gas calculation, by directly comparing the range of correlations that can be observed in harmonic and box traps near the BEC critical point.

In a homogeneous system near the critical point, the correlation length ξ diverges as illustrated in **a**. At a fixed temperature,

$$\xi/\lambda = A(|n - n_c|/n_c)^{-\nu},$$

where λ is the thermal wavelength, n_c the critical density, ν the critical exponent and A a non-universal prefactor; for the ideal-gas BEC transition[146] $n_c = 2.612/\lambda^3$, $\nu = 1$ and $A = 1/2.612$.

For a harmonically trapped gas with spatially uniform T, one can evaluate a spatially varying $\xi(r)$, where r is the distance from the trap center, within the LDA; that is, assuming that ξ at each r is the same as in a homogeneous system with density $n(r)$. However, this approach breaks down if $n(r=0)$ approaches n_c, because the deduced ξ becomes larger than the length scale over which n (and hence ξ itself) varies significantly. One can still, at the cost of reducing the experimental signal, focus on the central part of the cloud and assume that n is constant within some non-infinitesimal volume (as in refs. [70,71,73,147]). In reality, n and ξ vary within this region but one can still directly probe correlations on a length scale ℓ if $\xi(r) > \ell$ for all $r < \ell/2$; this approach was used in ref. [148].

Setting $n(r=0) = n_c$, assuming an isotropic potential $(1/2)m\omega^2 r^2$, and expanding the ideal-gas distribution[1] near $r=0$ gives $\xi(r)/\lambda \approx k_B T/(\hbar\omega) \times [2\pi r/\lambda]^{-1}$. Noting that

$$k_B T/(\hbar\omega) = (N/1.202)^{1/3},$$

where N is the total number of atoms in the trap and k_B the Boltzmann constant, in **b** we plot ξ/λ versus r/λ for different N (black lines). The intersects of these curves with the line $\xi = 2r$ (red) then give the achievable $\ell = 2r$ for a given N, irrespective of the choices of ω and corresponding T. Conversely, the atom number needed to directly observe correlations on ℓ in a harmonic trap is

$$N_{harm} = 1.202\,\pi^3(\ell/\lambda)^6, \quad (1)$$

shown by the red line in **c**. With a typical $N \approx 10^6$, one can reach only $\ell \approx 5\lambda$.

On the other hand, working with a box trap, one just needs a box of size ℓ and the corresponding atom number

$$N_{box} = n_c \ell^3 \approx 2.612 \times (\ell/\lambda)^3, \quad (2)$$

shown by the green line in **c**. In this case, the same $N \approx 10^6$ is sufficient for measurements up to $\ell \approx 70\lambda$.

For an interacting gas, for which[148–150] $\nu \approx 0.67$, one reaches similar conclusions. In this case, $N_{box} \propto (\ell/\lambda)^3$ is essentially the same, with just the prefactor ($\propto n_c/\lambda^3$) changing slightly, and one can estimate N_{harm} in various ways: still assuming ideal-gas $n(r)$ gives $N_{harm} \propto (\ell/\lambda)^{3+3/\nu} = (\ell/\lambda)^{7.5}$, whereas approximating $n(r)$ as a Gaussian gives $N_{harm} \propto (\ell/\lambda)^{3+3/(2\nu)} = (\ell/\lambda)^{5.25}$. In either case, one concludes that with the same atom number resources one can directly observe much-longer-range correlations in a box trap.

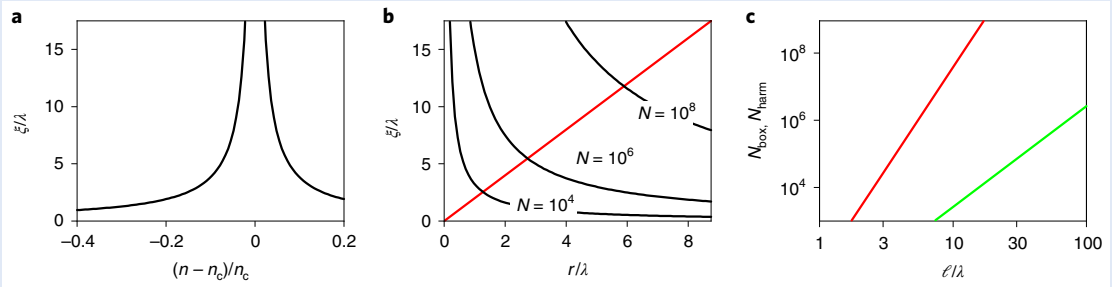

Another major topic for which homogeneous gases have distinct advantages is the critical behaviour near second-order phase transitions, where the range of correlations in the gas diverges (Fig. 4b and Box 2). This is fundamentally homogeneous-system physics and it is hard to study it in inhomogeneous systems, because the local density approximation (LDA) breaks down owing to the divergence of the correlation length. In a non-equilibrium context, dynamic crossing of such a transition results in causally disconnected domains that display different choices of the symmetry-breaking order parameter. The Kibble–Zurek theory[84,85] that describes these dynamics was originally developed specifically for homogeneous systems and its key assumption is that when it comes to the choice of the order parameter, all parts of the system have 'equal voting rights'[86,87]. Box-trap experiments have provided quantitative tests of the Kibble–Zurek predictions for how the domain size[37] and the resulting density of defects in the ordered state[15] depend on the quench rate (see also refs. [36,38,88] for ring-trap and optical-tweezer experiments).

A number of other non-equilibrium experiments have been made possible by different properties of homogeneous gases. The form of the excitation spectrum of a weakly interacting 1D Bose gas allowed the observation of recurrences in a closed quantum system[31,89] (Fig. 4c). A momentum-space study of an energy-quenched far-from-equilibrium 3D Bose gas revealed bidirectional universal scaling dynamics[90]. Finally, in a 3D Bose gas quenched to unitarity, the fact that all parts of a non-equilibrium homogeneous cloud evolved in the same way allowed the observation of universal loss and prethermalization dynamics[91,92].

Other box-trap-enabled experiments. Finally, box trapping and related technologies have also facilitated many experiments that are less directly related to the physics of homogeneous gases. One example of this is the discovery of a novel breather in a 2D Bose gas[33]; the breather shown in Fig. 4d is observed in a harmonic potential, but the initial state had to be prepared in a box trap[33]. Another similar example is the deterministic preparation of a Townes soliton in ref. [93] (see also refs. [94,95] for other observations of Townes solitons in box traps); this 2D soliton is an inhomogeneous ground state of the system, but its deterministic preparation started with a homogeneous gas and imprinting arbitrary density profiles using a DMD[96]. A different example of a practical advantage of box traps is the observation of the transition from an atomic to a molecular condensate[97]; in this case the creation of a (quasi-)equilibrium condensed gas of

unstable molecules was facilitated by the use of a 2D box trap to minimize losses and heating. Further examples of box-trap-enabled experiments include observation of the weak collapse of a condensate with attractive interactions[98] and the studies of the modulation instabilities that lead to emission of matter-wave jets, pattern formation and quasiparticle pair-production[99–102].

Outlook

The scientific exploitation of box-trapped quantum gases is still in its infancy, with many exciting possibilities for the future. The successful studies of phase-transition dynamics could be extended to the infinite-order BKT transition[103–107] and the bubble-nucleation dynamics associated with first-order transitions, including some believed to be relevant to the physics of the early Universe[108–111]. Another general area where box traps could offer great advantage is topological physics[112,113]; sharp boundaries could allow real-space studies of edge states[114], which have so far been observed in cold-atom systems exploiting synthetic dimensions associated with internal (spin) degrees of freedom[115–117]. It has also been predicted[118] that the supersolid phases of gases with strong dipolar interactions[119–124] should be qualitatively different in a box trap.

Further opportunities are offered by combining box traps with other trapping methods. For example, the combination of box traps and optical lattices has already facilitated the observation of long-range antiferromagnetic correlations[125], as well as studies of competing magnetic orders in the bilayer Hubbard model[126]. Further possibilities are suggested by the hybrid trap of ref. [17], which is box-like along two directions and harmonic along the third. In this case, the harmonic direction provides tuning of the local chemical potential, while probing the system along a perpendicular direction retains many of the advantages of box traps—at least as long as the LDA is valid. Such a set-up could be used to study interfaces between different phases of matter, and could also facilitate searches for exotic states that are expected to occur only in narrow regions of bulk phase diagrams; an important example of such a still-sought-for phase is the Fulde–Ferrell–Larkin–Ovchinikov superfluid[127–129].

Although the range of scientific possibilities is broad and exciting, we can already anticipate that some will also require further technological developments.

The first issue is that many interesting experiments are likely to require increasingly larger and closer-to-perfect box traps. This is particularly true for studies of critical phenomena (Box 2), and more generally long-range correlations. As an illustration, a paradigmatic problem for which current technology is insufficient is that of the critical temperature for Bose–Einstein condensation in an interacting homogeneous gas[130–135]. Critical fluctuations in a repulsively interacting gas are predicted to raise T_c above the ideal-gas value. However, in a harmonic trap, one observes the opposite[136–140]—the beyond-mean-field correlation shift of T_c is diminished because only a small fraction of the cloud is critical at T_c, and it is overpowered by a geometric mean-field effect[141] that reduces T_c. For a general power-law trap, $V(r) \propto r^p$ (Box 1), with increasing p the beyond-mean-field shift should be more pronounced and the mean-field one should diminish. Using an LDA estimate, we found that for the currently typical values $p \approx 10$ the two effects are still comparable, and that one needs $p \gtrsim 100$ to cleanly observe the beyond-mean-field correlation shift of T_c. We expect other fundamental correlation–physics problems to similarly create a moving target for tolerable box imperfections.

The second issue is that many exciting possibilities rely on specific features of different atomic species and their mixtures, but the methods for the levitation of gases in 3D box traps are generally species-specific. The simplest magnetic levitation[14] works (strictly speaking) only for single-component gases, but can work well enough for mixtures of species that have similar ratios of mass and magnetic moment[17]. For two spin states of the same isotope, rapid swapping of the spins of individual particles can be used to levitate them simultaneously even if the two magnetic moments are significantly different[142]. Optical levitation can also extend the possibilities further, to multiple species with similar ratios of mass and polarizability[39]. However, creating arbitrary homogeneous mixtures of different chemical elements, different isotopes or even just different spin states of the same isotope, remains an open challenge.

These two issues are in fact related, as even in single-species experiments the limitations for making the box traps larger and closer to uniform (with larger p values) are often related to the need to levitate particles with additional fields. An exciting possibility for the future would therefore be to send box-trap set-ups into space and perform many-body experiments in a microgravity environment[143–145].

Received: 14 June 2021; Accepted: 4 October 2021;
Published online: 7 December 2021

References

1. Dalfovo, F., Giorgini, S., Pitaevskii, L. P. & Stringari, S. Theory of Bose–Einstein condensation in trapped gases. *Rev. Mod. Phys.* **71**, 463–512 (1999).
2. Giorgini, S., Pitaevskii, L. P. & Stringari, S. Theory of ultracold atomic Fermi gases. *Rev. Mod. Phys.* **80**, 1215–1274 (2008).
3. Bloch, I., Dalibard, J. & Zwerger, W. Many-body physics with ultracold gases. *Rev. Mod. Phys.* **80**, 885–964 (2008).
4. Görlitz, A. et al. Realization of Bose–Einstein condensates in lower dimensions. *Phys. Rev. Lett.* **87**, 130402 (2001).
5. Andrews, M. R. et al. Observation of interference between two Bose condensates. *Science* **275**, 637–641 (1997).
6. Anderson, B. P. & Kasevich, M. A. Macroscopic quantum interference from atomic tunnel arrays. *Science* **282**, 1686 (1998).
7. Greiner, M., Bloch, I., Mandel, O., Hänsch, T. W. & Esslinger, T. Exploring phase coherence in a 2D lattice of Bose–Einstein condensates. *Phys. Rev. Lett.* **87**, 160405 (2001).
8. Bloch, I. Ultracold quantum gases in optical lattices. *Nat. Phys.* **1**, 23–30 (2005).
9. Jin, D. S., Ensher, J. R., Matthews, M. R., Wieman, C. E. & Cornell, E. A. Collective excitations of a Bose–Einstein condensate in a dilute gas. *Phys. Rev. Lett.* **77**, 420–423 (1996).
10. Mewes, M.-O. et al. Collective excitations of a Bose–Einstein condensate in a magnetic trap. *Phys. Rev. Lett.* **77**, 988–991 (1996).
11. Andrews, M. R. et al. Propagation of sound in a Bose–Einstein condensate. *Phys. Rev. Lett.* **79**, 553–556 (1997).
12. Stamper-Kurn, D. M. et al. Reversible formation of a Bose–Einstein condensate. *Phys. Rev. Lett.* **81**, 2194–2197 (1998).
13. Greiner, M., Mandel, M. O., Esslinger, T., Hänsch, T. & Bloch, I. Quantum phase transition from a superfluid to a Mott insulator in a gas of ultracold atoms. *Nature* **415**, 39–44 (2002).
14. Gaunt, A. L., Schmidutz, T. F., Gotlibovych, I., Smith, R. P. & Hadzibabic, Z. Bose–Einstein condensation of atoms in a uniform potential. *Phys. Rev. Lett.* **110**, 200406 (2013).
15. Chomaz, L. et al. Emergence of coherence via transverse condensation in a uniform quasi-two-dimensional Bose gas. *Nat. Commun.* **6**, 6162 (2015).
16. Tajik, M. et al. Designing arbitrary one-dimensional potentials on an atom chip. *Optics Express* **27**, 33474 (2019).
17. Mukherjee, B. et al. Homogeneous atomic Fermi gases. *Phys. Rev. Lett.* **118**, 123401 (2017).
18. Hueck, K. et al. Two-dimensional homogeneous Fermi gases. *Phys. Rev. Lett.* **120**, 060402 (2018).
19. Bause, R. et al. Collisions of ultracold molecules in bright and dark optical dipole traps. *Phys. Rev. Res.* **3**, 033013 (2021).
20. Navon, N., Gaunt, A. L., Smith, R. P. & Hadzibabic, Z. Emergence of a turbulent cascade in a quantum gas. *Nature* **539**, 72–75 (2016).
21. Ville, J. L. et al. Sound propagation in a uniform superfluid two-dimensional Bose gas. *Phys. Rev. Lett.* **121**, 145301 (2018).
22. Patel, P. B. et al. Universal sound diffusion in a strongly interacting Fermi gas. *Science* **370**, 1222–1226 (2020).
23. Baird, L., Wang, X., Roof, S. & Thomas, J. E. Measuring the hydrodynamic linear response of a unitary Fermi gas. *Phys. Rev. Lett.* **123**, 160402 (2019).
24. Garratt, S. J. et al. From single-particle excitations to sound waves in a box-trapped atomic Bose–Einstein condensate. *Phys. Rev. A* **99**, 021601 (2019).
25. Christodoulou, P. et al. Observation of first and second sound in a BKT superfluid. *Nature* **594**, 191–194 (2021).

26. Bohlen, M. et al. Sound propagation and quantum-limited damping in a two-dimensional Fermi gas. *Phys. Rev. Lett.* **124**, 240403 (2020).
27. Zhang, J. et al. Many-body decay of the gapped lowest excitation of a Bose–Einstein condensate. *Phys. Rev. Lett.* **126**, 060402 (2021).
28. Lopes, R. et al. Quantum depletion of a homogeneous Bose–Einstein condensate. *Phys. Rev. Lett.* **119**, 190404 (2017).
29. Biss, H. et al. Excitation spectrum and superfluid gap of an ultracold Fermi gas. Preprint at https://arxiv.org/abs/2105.09820 (2021).
30. Sobirey, L. et al. Comparing fermionic superfluids in two and three dimensions. Preprint at https://arxiv.org/abs/2106.11893 (2021).
31. Rauer, B. et al. Recurrences in an isolated quantum many-body system. *Science* **360**, 307–310 (2018).
32. Schmidutz, T. F. et al. Quantum Joule–Thomson effect in a saturated homogeneous Bose gas. *Phys. Rev. Lett.* **112**, 040403 (2014).
33. Saint-Jalm, R. et al. Dynamical symmetry and breathers in a two-dimensional Bose gas. *Phys. Rev. X* **9**, 021035 (2019).
34. Amico, L. et al. Roadmap on Atomtronics: State of the art and perspective. *AVS Quantum Sci.* **3**, 039201 (2021).
35. Kaufman, A. & Ni, K.-K. & Quantum science with optical tweezer arrays of ultracold atoms and molecules. *Nat. Phys.* https://doi.org/10.1038/s41567-021-01357-2 (2021).
36. Corman, L. et al. Quench-induced supercurrents in an annular Bose gas. *Phys. Rev. Lett.* **113**, 135302 (2014).
37. Navon, N., Gaunt, A. L., Smith, R. P. & Hadzibabic, Z. Critical dynamics of spontaneous symmetry breaking in a homogeneous Bose gas. *Science* **347**, 167–170 (2015).
38. Keesling, A. et al. Quantum Kibble–Zurek mechanism and critical dynamics on a programmable Rydberg simulator. *Nature* **568**, 207 (2019).
39. Shibata, K., Ikeda, H., Suzuki, R. & Hirano, T. Compensation of gravity on cold atoms by a linear optical potential. *Phys. Rev. Res.* **2**, 013068 (2020).
40. Gauthier, G. et al. Direct imaging of a digital-micromirror device for configurable microscopic optical potentials. *Optica* **3**, 1136–1143 (2016).
41. Gauthier, G. et al. in *Advances In Atomic, Molecular, and Optical Physics* Vol. 70, 1–101 (Academic, 2021).
42. Gaunt, A. L., *Degenerate Bose Gases: Tuning Interactions & Geometry* PhD thesis, Univ. Cambridge (2014).
43. Manek, I., Ovchinnikov, Y. B. & Grimm, R. Generation of a hollow laser beam for atom trapping using an axicon. *Opt. Comm.* **147**, 67–70 (1998).
44. Henderson, K., Ryu, C., MacCormick, C. & Boshier, M. G. Experimental demonstration of painting arbitrary and dynamic potentials for Bose–Einstein condensates. *N. J. Phys.* **11**, 043030 (2009).
45. Davidson, N., Lee, H. J., Adams, C. S., Kasevich, M. & Chu, S. Long atomic coherence times in an optical dipole trap. *Phys. Rev. Lett.* **74**, 1311 (1995).
46. Ozeri, R., Khaykovich, L. & Davidson, N. Long spin relaxation times in a single-beam blue-detuned optical trap. *Phys. Rev. A* **59**, R1750 (1999).
47. Friedman, N., Khaykovich, L., Ozeri, R. & Davidson, N. Compression of cold atoms to very high densities in a rotating-beam blue-detuned optical trap. *Phys. Rev. A* **61**, 031403 (2000).
48. Rychtarik, D., Engeser, B., Nägerl, H.-C. & Grimm, R. Two-dimensional Bose–Einstein condensate in an optical surface trap. *Phys. Rev. Lett.* **92**, 173003 (2004).
49. Meyrath, T. P., Schreck, F., Hanssen, J. L., Chuu, C.-S. & Raizen, M. G. Bose–Einstein condensate in a box. *Phys. Rev. A* **71**, 041604 (2005).
50. Van Es, J. et al. Box traps on an atom chip for one-dimensional quantum gases. *J. Phys. B* **43**, 155002 (2010).
51. Ville, J. L. et al. Loading and compression of a single two-dimensional Bose gas in an optical accordion. *Phys. Rev. A* **95**, 013632 (2017).
52. Anderson, B. P. & Kasevich, M. A. Spatial observation of Bose–Einstein condensation of ^{87}Rb in a confining potential. *Phys. Rev. A* **59**, R938–R941 (1999).
53. Truscott, A., Strecker, K., McAlexander, W., Partridge, G. & Hulet, R. G. Observation of Fermi pressure in a gas of trapped atoms. *Science* **291**, 2570–2572 (2001).
54. Tammuz, N. et al. Can a Bose gas be saturated? *Phys. Rev. Lett.* **106**, 230401 (2011).
55. Kothari, D. S. & Srivasava, B. N. Joule–Thomson effect and quantum statistics. *Nature* **140**, 970–971 (1937).
56. Tisza, L. Transport phenomena in helium II. *Nature* **141**, 913 (1938).
57. Landau, L. D. The theory of superfluidity of helium II. *Phys. Rev.* **60**, 356–358 (1941).
58. Berezinskii, V. L. Destruction of long-range order in one-dimensional and two-dimensional system possessing a continous symmetry group - II. Quantum systems. *Sov. Phys. JETP* **34**, 610 (1971).
59. Kosterlitz, J. M. & Thouless, D. J. Ordering, metastability and phase transitions in two dimensional systems. *J. Phys. C* **6**, 1181 (1973).
60. Nelson, D. R. & Kosterlitz, J. M. Universal jump in the superfluid density of two-dimensional superfluids. *Phys. Rev. Lett.* **39**, 1201–1205 (1977).
61. Luick, N. et al. An ideal Josephson junction in an ultracold two-dimensional Fermi gas. *Science* **369**, 89–91 (2020).
62. Sobirey, L. et al. Observation of superfluidity in a strongly correlated two-dimensional Fermi gas. *Science* **372**, 844–846 (2021).
63. Gauthier, G. et al. Quantitative acoustic models for superfluid circuits. *Phys. Rev. Lett.* **123**, 260402 (2019).
64. Gotlibovych, I. et al. Observing properties of an interacting homogeneous Bose–Einstein condensate: Heisenberg-limited momentum spread, interaction energy, and free-expansion dynamics. *Phys. Rev. A* **89**, 061604 (2014).
65. Lopes, R. et al. Quasiparticle energy in a strongly interacting homogeneous Bose–Einstein condensate. *Phys. Rev. Lett.* **118**, 210401 (2017).
66. Mukherjee, B. et al. Spectral response and contact of the unitary Fermi gas. *Phys. Rev. Lett.* **122**, 203402 (2019).
67. Yan, Z. et al. Boiling a unitary Fermi liquid. *Phys. Rev. Lett.* **122**, 093401 (2019).
68. Zou, Y.-Q. et al. Magnetic dipolar interaction between hyperfine clock states in a planar alkali Bose gas. *Phys. Rev. Lett.* **125**, 233604 (2020).
69. Zou, Y. et al. Tan's two-body contact across the superfluid transition of a planar Bose gas. *Nat. Commun.* **12**, 760 (2021).
70. Sagi, Y., Drake, T. E., Paudel, R. & Jin, D. S. Measurement of the homogeneous contact of a unitary Fermi gas. *Phys. Rev. Lett.* **109**, 220402 (2012).
71. Sagi, Y., Drake, T. E., Paudel, R., Chapurin, R. & Jin, D. S. Breakdown of the Fermi–liquid description for strongly interacting fermions. *Phys. Rev. Lett.* **114**, 075301 (2015).
72. Ota, M., Tajima, H., Hanai, R., Inotani, D. & Ohashi, Y. Local photoemission spectra and effects of spatial inhomogeneity in the BCS-BEC-crossover regime of a trapped ultracold Fermi gas. *Phys. Rev. A* **95**, 053623 (2017).
73. Carcy, C. et al. Contact and sum rules in a near-uniform Fermi gas at unitarity. *Phys. Rev. Lett.* **122**, 203401 (2019).
74. Kozuma, M. et al. Coherent splitting of Bose–Einstein condensed atoms with optically induced Bragg diffraction. *Phys. Rev. Lett.* **82**, 871–875 (1999).
75. Stenger, J. et al. Bragg spectroscopy of a Bose–Einstein condensate. *Phys. Rev. Lett.* **82**, 4569–4573 (1999).
76. Zakharov, V. E., L'vov, V. S. & Falkovich, G. *Kolmogorov Spectra of Turbulence* (Springer, 1992).
77. Navon, N. et al. Synthetic dissipation and cascade fluxes in a turbulent quantum gas. *Science* **366**, 382–385 (2019).
78. Gauthier, G. et al. Giant vortex clusters in a two-dimensional quantum fluid. *Science* **364**, 1264–1267 (2019).
79. Johnstone, S. P. et al. Evolution of large-scale flow from turbulence in a two-dimensional superfluid. *Science* **364**, 1267–1271 (2019).
80. Stockdale, O. R. et al. Universal dynamics in the expansion of vortex clusters in a dissipative two-dimensional superfluid. *Phys. Rev. Res.* **2**, 033138 (2020).
81. Reeves, M. T. et al. Emergence of off-axis equilibria in a quantum vortex gas. Preprint at https://arxiv.org/abs/2010.10049 (2020).
82. Onsager, L. Statistical hydrodynamics. *Nuovo Cimento* **6**, 279–287 (1949).
83. Kwon, W. J. et al. Sound emission and annihilations in a programmable quantum vortex collider. Preprint at https://arxiv.org/abs/2105.15180 (2021).
84. Kibble, T. W. B. Topology of cosmic domains and strings. *J. Phys. A* **9**, 1387–1398 (1976).
85. Zurek, W. H. Cosmological experiments in superfluid helium? *Nature* **317**, 505–508 (1985).
86. del Campo, A. & Zurek, W. H. Universality of phase transition dynamics: topological defects from symmetry breaking. *Int. J. Mod. Phys. A* **29**, 1430018 (2014).
87. Beugnon, J. & Navon, N. Exploring the Kibble–Zurek mechanism with homogeneous Bose gases. *J. Phys. B* **50**, 022002 (2017).
88. Aidelsburger, M. et al. Relaxation dynamics in the merging of *n* independent condensates. *Phys. Rev. Lett.* **119**, 190403 (2017).
89. Schweigler, T. et al. Decay and recurrence of non-Gaussian correlations in a quantum many-body system. *Nat. Phys.* **17**, 559–563 (2021).
90. Glidden, J. A. P. et al. Bidirectional dynamic scaling in an isolated Bose gas far from equilibrium. *Nat. Phys.* **17**, 457–461 (2021).
91. Eigen, C. et al. Universal scaling laws in the dynamics of a homogeneous unitary Bose gas. *Phys. Rev. Lett.* **119**, 250404 (2017).
92. Eigen, C. et al. Universal prethermal dynamics of Bose gases quenched to unitarity. *Nature* **563**, 221–224 (2018).
93. Bakkali-Hassani, B. et al. Realization of a Townes soliton in a two-component planar Bose gas. *Phys. Rev. Lett.* **127**, 023603 (2021).
94. Chen and C.-L. Hung, C.-A. Observation of universal quench dynamics and Townes soliton formation from modulational instability in two-dimensional Bose gases. *Phys. Rev. Lett.* **125**, 250401 (2020).
95. Chen, C.-A. & Hung, C.-L. Observation of scale invariance in two-dimensional matter-wave Townes solitons. *Phys. Rev. Lett.* **127**, 023604 (2021).
96. Zou, Y.-Q. et al. Optical control of the density and spin spatial profiles of a planar Bose gas. *J. Phys. B* **54**, 08LT01 (2021).

97. Zhang, Z., Chen, L., Yao, K. & Chin, C. Transition from an atomic to a molecular Bose–Einstein condensate. *Nature* **592**, 708–711 (2021).
98. Eigen, C. et al. Observation of weak collapse in a Bose–Einstein condensate. *Phys. Rev. X* **6**, 041058 (2016).
99. Clark, L. W., Gaj, A., Feng, L. & Chin, C. Collective emission of matter-wave jets from driven Bose–Einstein condensates. *Nature* **551**, 356–359 (2017).
100. Fu, H. et al. Density waves and jet emission asymmetry in Bose fireworks. *Phys. Rev. Lett.* **121**, 243001 (2018).
101. Zhang, Z., Yao, K.-X., Feng, L., Hu, J. & Chin, C. Pattern formation in a driven Bose–Einstein condensate. *Nat. Phys.* **16**, 652–656 (2020).
102. Chen, C.-A., Khlebnikov, S. & Hung, C.-L. Observation of quasiparticle pair production and quantum entanglement in atomic quantum gases quenched to an attractive interaction. *Phys. Rev. Lett.* **127**, 060404 (2021).
103. Mathey, L. & Polkovnikov, A. Light cone dynamics and reverse Kibble–Zurek mechanism in two-dimensional superfluids following a quantum quench. *Phys. Rev. A* **81**, 033605 (2010).
104. Jelić, A. & Cugliandolo, L. F. Quench dynamics of the 2d XY model. *J. Stat. Mech.* **2011**, 02032 (2011).
105. Mathey, L., Günter, K. J., Dalibard, J. & Polkovnikov, A. Dynamic Kosterlitz–Thouless transition in two-dimensional Bose mixtures of ultracold atoms. *Phys. Rev. A* **95**, 053630 (2017).
106. Comaron, P., Larcher, F., Dalfovo, F. & Proukakis, N. P. Quench dynamics of an ultracold two-dimensional Bose gas. *Phys. Rev. A* **100**, 033618 (2019).
107. Brown, K., Bland, T., Comaron, P. & Proukakis, N. P. Periodic quenches across the Berezinskii-Kosterlitz–Thouless phase transition. *Phys. Rev. Res.* **3**, 013097 (2021).
108. Fialko, O., Opanchuk, B., Sidorov, A. I., Drummond, P. D. & Brand, J. Fate of the false vacuum: towards realization with ultra-cold atoms. *Europhys. Lett.* **110**, 56001 (2015).
109. Braden, J., Johnson, M. C., Peiris, H. V. & Weinfurtner, S. Towards the cold atom analog false vacuum. *J. High Energy Phys.* **2018**, 14 (2018).
110. Braden, J., Johnson, M. C., Peiris, H. V., Pontzen, A. & Weinfurtner, S. Nonlinear dynamics of the cold atom analog false vacuum. *J. High Energy Phys.* **2019**, 174 (2019).
111. Billam, T. P., Gregory, R., Michel, F. & Moss, I. G. Simulating seeded vacuum decay in a cold atom system. *Phys. Rev. D* **100**, 065016 (2019).
112. Goldman, N., Budich, J. C. & Zoller, P. Topological quantum matter with ultracold gases in optical lattices. *Nat. Phys.* **12**, 639–645 (2016).
113. Ozawa, T. et al. Topological photonics. *Rev. Mod. Phys.* **91**, 015006 (2019).
114. Fletcher, R. J. et al. Geometric squeezing into the lowest Landau level. *Science* **372**, 1318–1322 (2021).
115. Mancini, M. et al. Observation of chiral edge states with neutral fermions in synthetic Hall ribbons. *Science* **349**, 1510–1513 (2015).
116. Stuhl, B. K., Lu, H. I., Aycock, L. M., Genkina, D. & Spielman, I. B. Visualizing edge states with an atomic Bose gas in the quantum Hall regime. *Science* **349**, 1514–1518 (2015).
117. Chalopin, T. et al. Probing chiral edge dynamics and bulk topology of a synthetic Hall system. *Nat. Phys.* **16**, 1017–1021 (2020).
118. Roccuzzo, S. M., Stringari, S. & Recati, A. Supersolid edge and bulk phases of a dipolar quantum gas in a box. Preprint at https://arxiv.org/abs/2104.01068 (2021).
119. Böttcher, F. et al. Transient supersolid properties in an array of dipolar quantum droplets. *Phys. Rev. X* **9**, 011051 (2019).
120. Tanzi, L. et al. Observation of a dipolar quantum gas with metastable supersolid properties. *Phys. Rev. Lett.* **122**, 130405 (2019).
121. Chomaz, L. et al. Long-lived and transient supersolid behaviors in dipolar quantum gases. *Phys. Rev. X* **9**, 021012 (2019).
122. Norcia, M. A. et al. Two-dimensional supersolidity in a dipolar quantum gas. *Nature* **596**, 357–361 (2021).
123. Hertkorn, J. et al. Supersolidity in two-dimensional trapped dipolar droplet arrays. *Phys. Rev. Lett.* **127**, 155301 (2021).
124. Böttcher, F. et al. New states of matter with fine-tuned interactions: quantum droplets and dipolar supersolids. *Rep. Progr. Phys.* **84**, 012403 (2021).
125. Mazurenko, A. et al. A cold-atom Fermi–Hubbard antiferromagnet. *Nature* **545**, 462–466 (2017).
126. Gall, M., Wurz, N., Samland, J., Chan, C. F. & Köhl, M. Competing magnetic orders in a bilayer Hubbard model with ultracold atoms. *Nature* **589**, 40–43 (2021).
127. Fulde, P. & Ferrell, R. A. Superconductivity in a strong spin-exchange field. *Phys. Rev.* **135**, A550–A563 (1964).
128. Larkin, A. I. & Ovchinnikov, Y. N. Nonuniform state of superconductors. *Zh. Eksp. Teor. Fiz.* **47**, 1136–1146 (1964).
129. Kinnunen, J. J., Baarsma, J. E., Martikainen, J.-P. & Törmä, P. The Fulde–Ferrell–Larkin–Ovchinnikov state for ultracold fermions in lattice and harmonic potentials: a review. *Rep. Progr. Phys.* **81**, 046401 (2018).
130. Lee, T. D. & Yang, C. N. Many-body problem in quantum mechanics and quantum statistical mechanics. *Phys. Rev.* **105**, 1119–1120 (1957).
131. Reppy, J. D. et al. Density dependence of the transition temperature in a homogeneous Bose–Einstein condensate. *Phys. Rev. Lett.* **84**, 2060–2063 (2000).
132. Arnold, P. & Moore, G. BEC transition temperature of a dilute homogeneous imperfect Bose gas. *Phys. Rev. Lett.* **87**, 120401 (2001).
133. Kashurnikov, V. A., Prokof'ev, N. V. & Svistunov, B. V. Critical temperature shift in weakly interacting Bose gas. *Phys. Rev. Lett.* **87**, 120402 (2001).
134. Andersen, J. O. Theory of the weakly interacting Bose gas. *Rev. Mod. Phys.* **76**, 599–639 (2004).
135. Holzmann, M., Fuchs, J.-N., Baym, G. A., Blaizot, J.-P. & Laloë, F. Bose Einstein transition temperature in a dilute repulsive gas. *C. R. Phys.* **5**, 21–37 (2004).
136. Ensher, J. R., Jin, D. S., Matthews, M. R., Wieman, C. E. & Cornell, E. A. Bose–Einstein condensation in a dilute gas: measurement of energy and ground-state occupation. *Phys. Rev. Lett.* **77**, 4984–4987 (1996).
137. Gerbier, F. et al. Critical temperature of a trapped, weakly interacting Bose gas. *Phys. Rev. Lett.* **92**, 030405 (2004).
138. Meppelink, R. et al. Thermodynamics of Bose–Einstein-condensed clouds using phase-contrast imaging. *Phys. Rev. A* **81**, 053632 (2010).
139. Smith, R. P., Campbell, R. L. D., Tammuz, N. & Hadzibabic, Z. Effects of interactions on the critical temperature of a trapped Bose gas. *Phys. Rev. Lett.* **106**, 250403 (2011a).
140. Smith, R. P., Tammuz, N., Campbell, R. L. D., Holzmann, M. & Hadzibabic, Z. Condensed fraction of an atomic Bose gas induced by critical correlations. *Phys. Rev. Lett.* **107**, 190403 (2011).
141. Giorgini, S., Pitaevskii, L. P. & Stringari, S. Condensate fraction and critical temperature of a trapped interacting Bose gas. *Phys. Rev. A* **54**, R4633–R4636 (1996).
142. Shkedrov, C., Menashes, M., Ness, G., Vainbaum, A. & Sagi, Y. Absence of heating in a uniform Fermi gas created by periodic driving. Preprint at https://arxiv.org/abs/2102.09506 (2021).
143. Becker, D. et al. Space-borne Bose–Einstein condensation for precision interferometry. *Nature* **562**, 391–395 (2018).
144. Aveline, D. C. et al. Observation of Bose–Einstein condensates in an Earth-orbiting research lab. *Nature* **582**, 193–197 (2020).
145. Frye, K. et al. The Bose–Einstein condensate and cold atom laboratory. *EPJ Quantum Technol.* **8**, 1–38 (2021).
146. Huang, K. *Statistical Mechanics* (Wiley, 1987).
147. Drake, T. E. et al. Direct observation of the Fermi surface in an ultracold atomic gas. *Phys. Rev. A* **86**, 031601 (2012).
148. Donner, T. et al. Critical behavior of a trapped interacting Bose gas. *Science* **315**, 1556–1558 (2007).
149. Campostrini, M., Hasenbusch, M., Pelissetto, A. & Vicari, E. Theoretical estimates of the critical exponents of the superfluid transition in ^{4}He by lattice methods. *Phys. Rev. B* **74**, 144506 (2006).
150. Burovski, E., Prokof'ev, N., Svistunov, B. & Troyer, M. Critical temperature and thermodynamics of attractive fermions at unitarity. *Phys. Rev. Lett.* **96**, 160402 (2006).

Acknowledgements

We thank C. Eigen for help in the preparation of the figures and critical reading of the manuscript. We also thank R. Lopes and S. Nascimbene for comments on the manuscript, and M. Zwierlein, P. Patel, B. Mukherjee, J. Beugnon, J. Dalibard, R. Saint-Jalm, H. Biss, T. Lompe and H. Moritz for sharing their data. This work was supported by the EPSRC (grant numbers EP/N011759/1, EP/P009565/1 and EP/T019913/1), ERC (QBox), QuantERA (NAQUAS, EPSRC grant number EP/R043396/1), NSF CAREER (grant number 1945324) and DARPA (grant number 00010372). N.N. acknowledges support from the David and Lucile Packard Foundation, and the Alfred P. Sloan Foundation. R.P.S. acknowledges support from the Royal Society. Z.H. acknowledges support from the Royal Society Wolfson Fellowship.

Competing interests

The authors declare no competing interests.

Additional information

Correspondence should be addressed to Zoran Hadzibabic.

Peer review information *Nature Physics* thanks the anonymous reviewers for their contribution to the peer review of this work.